Experimental evidence for a natural parity state in ^{26}Mg and its impact on the production of neutrons for the *s* process

C. Ugalde,* A. E. Champagne, S. Daigle, C. Iliadis, R. Longland, J. R. Newton, and E. Osenbaugh-Stewart
Department of Physics and Astronomy, University of North Carolina, Chapel Hill, North Carolina 27599, USA and Triangle Universities Nuclear Laboratory, Durham, North Carolina 27708, USA

J. A. Clark, C. Deibel, A. Parikh,† P. D. Parker, and C. Wrede
Wright Nuclear Structure Laboratory, Yale University, New Haven, Connecticut 06520, USA
(Received 28 April 2007; published 9 August 2007)

We have studied natural parity states in ^{26}Mg via the ^{22}Ne(^{6}Li, d)^{26}Mg reaction. Our method significantly improves the energy resolution of previous experiments and, as a result, we report the observation of a natural parity state in ^{26}Mg. Possible spin-parity assignments are suggested on the basis of published γ-ray decay experiments. The stellar rate of the ^{22}Ne(α, γ)^{26}Mg reaction is reduced and may give rise to an increase in the production of *s*-process neutrons via the ^{22}Ne(α, n)^{25}Mg reaction.

DOI: 10.1103/PhysRevC.76.025802 PACS number(s): 26.20.+f, 27.30.+t, 23.20.Lv, 25.70.Hi

I. INTRODUCTION

The ^{22}Ne(α, n)^{25}Mg reaction is regarded as the main neutron source for the *s* process in core He-burning massive stars [1] and is of relevance in He-shell burning in AGB stars [2]. Our current understanding of its rate is one of the most important sources of uncertainty in the nucleosynthesis of heavy elements.

The species ^{22}Ne is produced in helium-rich environments from ^{14}N, a product of the CNO cycle, via ^{14}N(α, γ)^{18}F($\beta^+\nu$)^{18}O(α, γ)^{22}Ne. The production of neutrons by α-particle capture on ^{22}Ne occurs through a resonant process involving the formation of the ^{26}Mg compound nucleus in an excitation range of high level density. The populated resonant levels decay by neutron emission to the ground state of ^{25}Mg. Figure 1 shows both the formation channel (open above $E_x = 10{,}614.78 \pm 0.03$ keV) and the outgoing neutron channel (open above $E_x = 11{,}093.07 \pm 0.04$ keV).

The ^{22}Ne(α, γ)^{26}Mg reaction competes with the ^{22}Ne(α, n)^{25}Mg process [3] above the neutron threshold. At temperatures of relevance to the main and weak components of the *s* process, the neutron yield is defined by both the abundance of ^{22}Ne and the branching ratio between the competing γ-ray and neutron exit channels [4]. Direct measurements of both processes have been reported by several groups for $E_\alpha^{\rm lab} > 800$ keV (for example, see [5–9] and other references therein). However, due to the Coulomb barrier, the cross section remains uncertain for lower energies. A direct measurement for $E_\alpha^{\rm lab} < 800$ keV still needs to be done.

There is only scarce information on levels of ^{26}Mg between the α-particle and neutron thresholds. Giesen *et al*. [7] report two natural parity resonances [at $E_x = 10.694(20)$ MeV and $E_x = 10.949(25)$ MeV] in their ^{22}Ne(^{6}Li, d)^{26}Mg experiments. As discussed by Karakas *et al*. [10], the main source of uncertainty in the rate for the ^{22}Ne(α, γ)^{26}Mg reaction at these energies results from the unknown spin of the ^{26}Mg state at $E_x = 10.949(25)$ MeV. However, in their calculation of the rate, Karakas *et al*. have considered only two states while more than 20 levels are listed in the compilation of Endt [11] for excitation energies between the α-particle and neutron emission thresholds. A detailed study of levels in ^{26}Mg and their spins and parities at these energies is urgently needed. Here we report the first experimental step toward a complete understanding of the reaction rate at stellar temperatures.

Both ^{22}Ne and ^{4}He have a ground state with $J^\pi = 0^+$. Thus, preferentially natural parity states in ^{26}Mg can be populated via the ^{4}He+^{22}Ne process [12]. We studied the astrophysically relevant natural parity states in ^{26}Mg between $E_x = 10615$ keV and $E_x = 11093$ keV via the ^{22}Ne(^{6}Li, d)^{26}Mg reaction, which preferentially populates natural parity states for direct α-particle transfer [13].

II. EXPERIMENT

Five ^{22}Ne targets were prepared by implanting ^{22}Ne into 40 μg/cm^2, 99.9% ^{12}C-enriched foils. The foils were floated from glass slides in deionized water and mounted onto aluminum frames. It is thought that the mechanical stability of thin foils can be improved by exposing them to an intense burst of light [14]. We flashed the unimplanted foils with a photographic strobe and observed their slackening. The ^{22}Ne beam was produced by the 200 keV Eaton Ion Implanter at the University of North Carolina; two energies (20 keV and 35 keV) were used to implant both sides of the foils. ^{22}Ne was implanted in this way to achieve a total density of 19–22 $\times 10^{16}$ atoms/cm^2 ($\sim$7 μg/cm^2). The dose of implanted ions was estimated by integrating the beam current at the target, which together with the beam stop and the implantation chamber, acted as a Faraday cup. Secondary electrons were suppressed with a negative voltage applied to a copper pipe placed in front of the target and coaxial to the beam.

*cugalde@unc.edu
†Current address: Departament de Física i Enginyeria Nuclear, Universitat Politécnica de Catalunya, Barcelona, Spain.

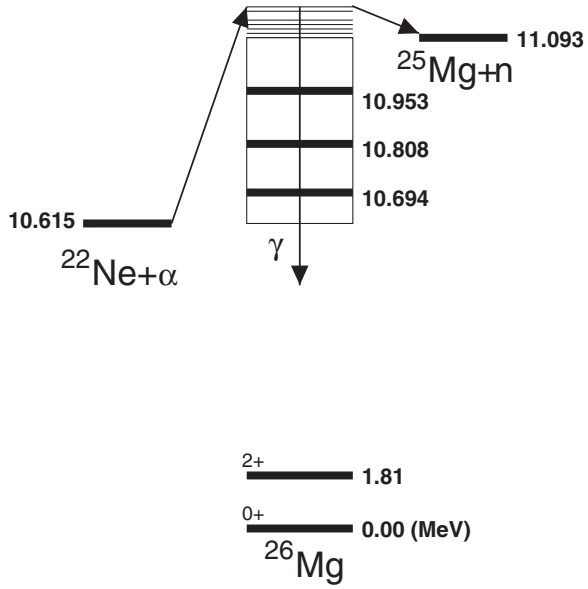

FIG. 1. Level scheme (not drawn to scale) of ^{26}Mg showing the ^{22}Ne+α entrance channel and the two competing exit channels ^{25}Mg+n and ^{26}Mg+γ. The levels of interest to this work (all below the neutron threshold) are shown. Note the negative Q-value ($Q = -478.3 \pm 0.04$ keV) for the ^{22}Ne(α, n)^{25}Mg process.

The copper pipe was cooled with liquid nitrogen to prevent natural carbon build up on the targets. It was important to keep ^{13}C contamination of the targets to a minimum because deuterons from the ^{13}C(^{6}Li, d)^{17}O reaction would have posed a major source of background in our ^{22}Ne(^{6}Li, d)^{26}Mg spectra. An additional source of background could have been ^{20}Ne from the ion source at the implanter. The natural neon gas used to produce the beam was mass analyzed using a magnet with a mass resolution better than $\Delta M/M = 0.01$ allowed us to get an excellent separation of ^{22}Ne and ^{20}Ne. The ^{22}Ne beam current was kept below 400 nA to minimize heating of the carbon foils.

Both the ^{22}Ne(^{6}Li, d)^{26}Mg experiment and analysis of the target composition were performed with a ^{6}Li beam produced by the Wright Nuclear Structure Laboratory ESTU Tandem van de Graaff accelerator at Yale University. The reaction products were momentum-separated with the Enge split-pole spectrometer and detected at the focal plane with a position-sensitive gas ionization chamber and a scintillator [15].

The detector setup allowed us to separate different particle groups by means of the magnetic rigidity ($B\rho$), the energy loss (ΔE) measured from the cathode and the residual energy (E) deposited at the scintillator. The magnetic rigidity ($B\rho$) was derived from independent position signals along two parallel wires (front wire and rear wire). The horizontal acceptance was $\pm$10.7 mrad, which corresponded to the minimum aperture available.

The target content analysis was performed with a 7.7 MeV ^{6}Li beam. To calibrate the elastic scattering position spectrum as a function of mass, we used a target consisting of a SiO_2 layer deposited on a 40 μg/cm^2 natural carbon substrate. Elastic scattered ^{6}Li off the target was observed in three major groups, each corresponding to ^{12}C, ^{16}O, and ^{28}Si. A ^{22}Ne-implanted and a nonimplanted ^{12}C foil were exposed to a ^{6}Li beam as well (see Fig. 2).

The (^{6}Li, d) experiment was performed with a 30 MeV ^{6}Li beam. We took spectra with the nonimplanted target for magnetic rigidity calibration purposes and for comparison with the ^{22}Ne-implanted target. Because the cross section is expected to be larger at small scattering angles, we placed the spectrometer at 6° in the laboratory. The spectrometer field was set to center the deuterons from the ^{12}C(^{6}Li, d)^{16}O reaction at the position spectrum.

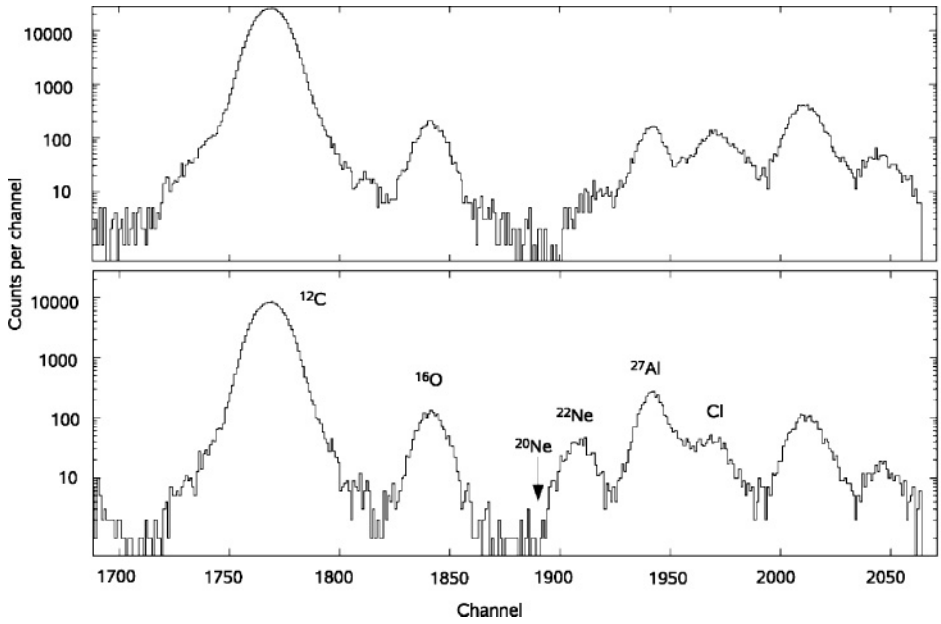

FIG. 2. Elastic scattering off a nonimplanted ^{12}C substrate (upper panel) and off a ^{22}Ne-implanted ^{12}C substrate (lower panel). The arrow shows the position where contaminating ^{20}Ne would have appeared.

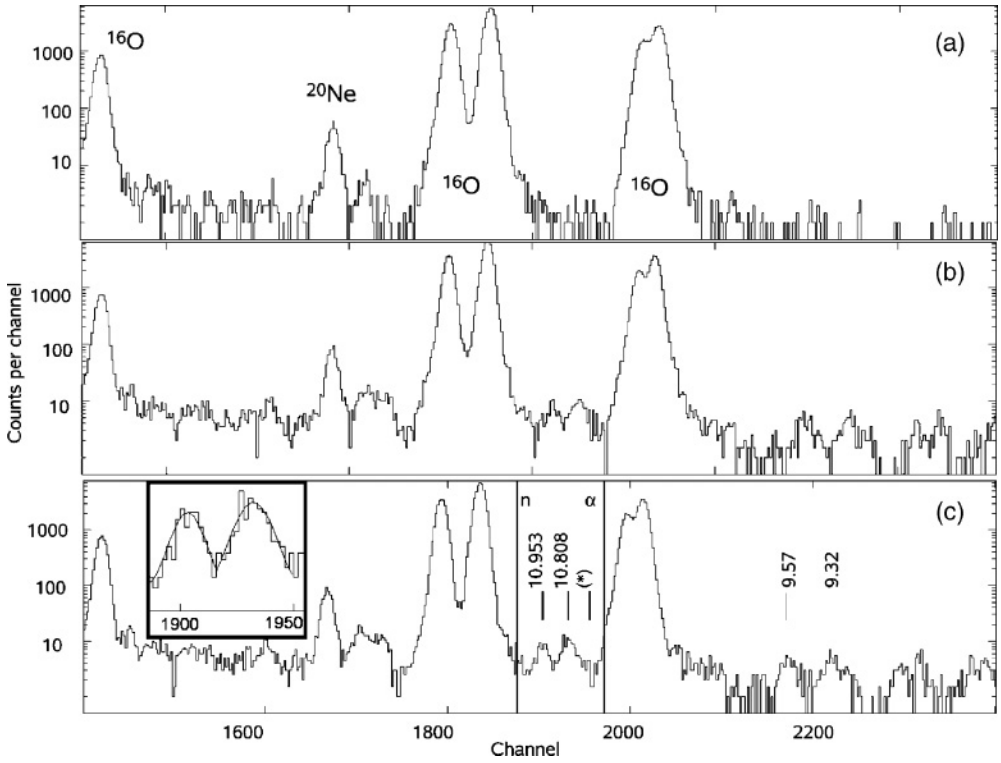

FIG. 3. Deuteron position spectra for $\theta_{\rm lab} = 6^\circ$. (a) The top panel shows the deuterons from the ^{12}C substrate. Six groups are observed and correspond, from left to right, to the $E_x = 8.8719(5)$ MeV state in ^{16}O [from ^{12}C(^{6}Li, d)^{16}O], the $E_x = 5.6214(17)$ MeV state in ^{20}Ne [from ^{16}O(^{6}Li, d)^{20}Ne], the $E_x = 7.11685(14)$ and 6.9171(6) MeV doublet in ^{16}O, and the $E_x = 6.12989(4)$ and 6.0494(10) MeV doublet in ^{16}O, both from ^{12}C(^{6}Li, d)^{16}O. (b) The middle panel shows the deuteron front position spectrum from a ^{22}Ne-implanted ^{12}C substrate. The energy region of interest in this work is the window located between the two ^{16}O doublets. Deuteron groups not observed with the ^{12}C target are seen here. (c) The lower panel shows the deuteron spectrum after reconstructing the focal plane for the ^{22}Ne-implanted ^{12}C substrate (see Sec. III). The energies of some of the observed ^{26}Mg states are shown. The two vertical lines correspond, from left to right, to the positions of the neutron and α-particle thresholds. The arrow labeled with an asterisk (*) corresponds to $E_x = 10.694$ MeV. A state was not observed at this energy and angle (see text for discussion). The inset shows the Gaussian fits to the two peaks in the region between the neutron and α-particle thresholds.

We acquired deuteron position spectra with an average beam current of 80 pnA with the ^{22}Ne target and a total solid angle of 1.5 msr. The result is shown in Fig. 3. The energy region of interest for deuteron groups corresponding to ^{26}Mg states is located between the two ^{16}O doublets. Deuteron groups unobserved with the ^{12}C target appear both inside and outside the region of interest.

III. ANALYSIS AND RESULTS

Although the detector was positioned so that the focal plane coincided nominally with the front wire, the two independent position measurements allowed us to more accurately locate the true focal plane by reconstructing the particle trajectories [16], thereby improving the position resolution. Let P_1 and P_2 be the positions measured at the front and rear wire, respectively, and S the distance between the wires ($S = 2.5$ cm). The trajectory (x, y) of particles traveling in a plane parallel to the two wires is described by the relation

$$(P_1 - P_2)y + Sx - P_2 S = 0. \qquad (1)$$

On the other hand, the (x, y) equation for the focal plane is

$$\frac{x}{(1+\cot^2\alpha)^{\frac{1}{2}}} + \frac{y}{(1+\tan^2\alpha)^{\frac{1}{2}}} - H = 0, \qquad (2)$$

where α is the angle between the focal plane and the front wire, and H is the distance from the focal plane to the origin $(0, 0)$. Solving (x, y) simultaneously for the two equations one gets the position of the particles at the focal plane (see Fig. 4). The best position resolution was obtained for $S/H = 2$. The resulting spectrum is shown in Fig. 3(c); here the energy resolution improved from 80 keV to 58 keV, as measured for the ^{16}O peak at $E_x = 7.12$ MeV.

The S/H value was chosen to optimize the resolution of the ^{16}O peaks in the position spectrum. The main source of background was the ^{12}C substrate in the target, as can be noted by comparing panels (a) and (c) in Fig. 3. Therefore, the best peak to background ratio for the ^{26}Mg states was obtained by focusing on the ^{16}O peaks instead of the ^{26}Mg states themselves. Nevertheless, the width of ^{26}Mg peaks for $S/H = 2$ was still within 5% of the optimized value for the focused ^{26}Mg peaks ($S/H = 1.67$). The width observed for the ^{26}Mg peaks is listed in Table I.

TABLE I. States observed in this work.

Centroid (channel)	E_x (MeV)	E_d[c] (MeV)	Nucleus	Peak width (keV)
1419.6(10)	8.8719(5)[a]	24.147(2)	^{16}O	
1667.1(10)	5.7877(26)[a]	25.450(11)	^{20}Ne	
1792.4(15)	7.11685(14)[a]	26.122(1)	^{16}O	
1834.4(10)	6.9171(6)[a]	26.345(2)	^{16}O	
1903.2(50)	10.953(25)[b]	26.719(61)	^{26}Mg	58(16)
1931.8(40)	10.808(20)[b]	26.872(50)	^{26}Mg	69(16)
1996.8(20)	6.12989(4)[a]	27.224(1)	^{16}O	
2012.6(20)	6.0494(10)[a]	27.314(5)	^{16}O	
2173.5(80)	9.57(4)[b]	28.19(12)	^{26}Mg	117(15)
2221.4(110)	9.32(6)[b]	28.46(18)	^{26}Mg	172(20)

[a]From [17], used as calibration peaks.
[b]This work.
[c]Deuteron energy, as calculated from a kinematic analysis.

The origin of the deuteron groups observed with the ^{22}Ne target was established on the basis of a target content analysis via ^{6}Li elastic scattering. The target content analysis was performed by moving the spectrometer to 20° in the laboratory frame and reducing the magnetic field to 7.7 kG, so that elastically scattered ^{6}Li ions were centered at the front position spectrum. The results for both the nonimplanted and ^{22}Ne-implanted ^{12}C substrates are shown in Fig. 2. The major peak appearing in the spectra corresponds to the ground state in ^{12}C. Other elastic scattering groups were also identified. A comparison between these two elastic scattering spectra shows that the only group observed in the ^{22}Ne-implanted target and not observed in the nonimplanted target is that corresponding to ^{22}Ne. The position where ^{20}Ne contamination from the implantation process would have appeared is marked as well. From Fig. 2 it is clear that ^{27}Al is also increased relative to the ^{12}C group between both targets (probably as a result of the implantation process). Therefore, we compared the deuteron spectrum obtained from an ^{27}Al target with that of the ^{22}Ne-implanted target. We scaled the background

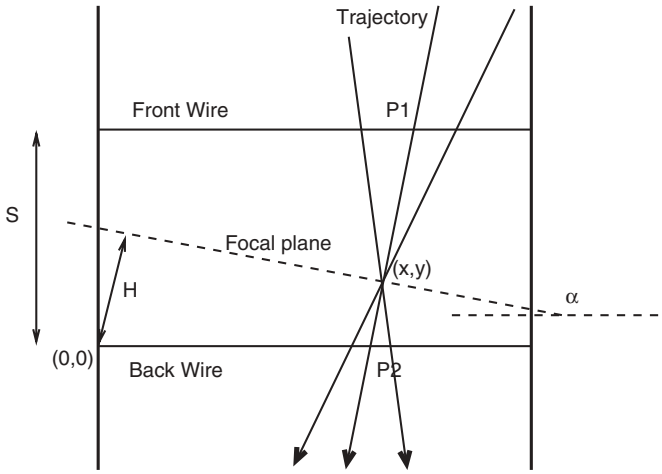

FIG. 4. Deuteron trajectory and focal plane diagram (adapted from [16]).

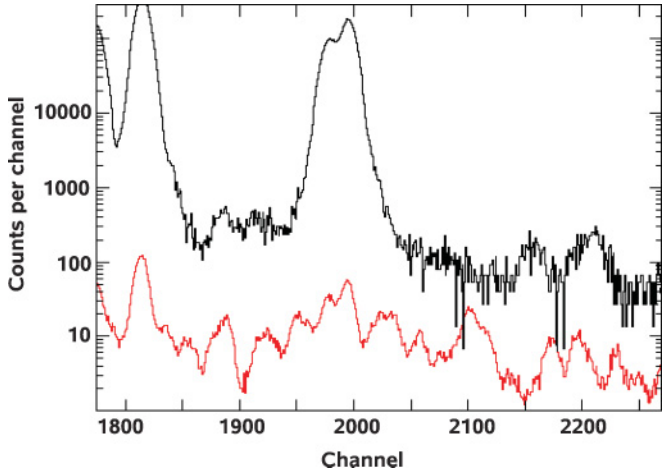

FIG. 5. (Color online) Comparison between spectra obtained with both a ^{22}Ne-implanted target (black curve) and an ^{27}Al target (red curve). The yield for the ^{27}Al target was renormalized to match the relative accumulated charge on the ^{22}Ne-implanted target and the relative ^{27}Al content in the targets, as measured with elastic scattering of ^{6}Li. Both spectra were taken with a beam energy of 30 MeV and the spectrometer placed at 6°.

with the ^{27}Al content determined via elastic scattering in the ^{22}Ne-implanted target (see Fig. 5 for a content-normalized comparison between spectra from both targets). We concluded the peaks observed between the two ^{16}O doublets originated from the ^{22}Ne(^{6}Li, d)^{26}Mg reaction, with a contribution of 5% from ^{27}Al to the area under the peaks.

From the position spectrum, a magnetic rigidity and an excitation energy calibration can be obtained by assuming a polynomial relation for the radius of curvature ρ. This requires that at least three peaks be unambiguously identified. Here we used six states that were populated via the ^{12}C(^{6}Li, d)^{16}O and ^{16}O(^{6}Li, d)^{20}Ne reactions (see Table I).

The position of peaks observed was determined by fitting with a Gaussian template. The error bars of centroid positions were determined by sampling the area and width of the Gaussian determined by minimizing the value of χ^2 for the fit, within error bars. A Monte Carlo sampling produced a set of centroid positions that determined the size of error bars. Table I shows the centroids of the fitted peaks and the published excitation energies [17] for the six calibration peaks. We fitted ρ, the deuteron trajectory's radius of curvature, as a function of the front wire position P_1 with an expression of the type

$$\rho(P_1) = a_0 + a_1(P_1 - P_1[0]) + \cdots. \tag{3}$$

Here the a_i's are the parameters of the fit. We found that the best fit ($\chi^2/N = 0.1$, where $N = 3$ is the number of degrees of freedom) was obtained with a polynomial of degree 2. Finally, the excitation energy of ^{26}Mg states was computed from ρ with a kinematic analysis. The error bars include contributions from the uncertainty in the position of the centroid of the peaks and from the energy calibration.

IV. DISCUSSION

The recent calculation of the rate for the ^{22}Ne$(\alpha,\gamma)^{26}$Mg reaction [10] includes contributions from two ^{26}Mg states below the neutron threshold. The largest source of uncertainty is from the $E_x = 10.949(25)$ MeV state; a second state at $E_x = 10.694(20)$ MeV ($E_{\text{c.m.}} = 0.078$ MeV) has a negligible effect on the rate, as it is located too far below the Gamow window for He-burning temperatures (the window spans from $E_{\text{c.m.}} = 0.36$ to 0.57 MeV at $T = 2.0 \times 10^8$ K). Both states were observed by Giesen *et al.* [7] using the ^{22}Ne$(^6$Li$, d)^{26}$Mg reaction. However, we find evidence that their $E_x = 10.949(25)$ MeV state corresponds to at least two states in ^{26}Mg.

Four ^{26}Mg states were identified in this experiment (see Table I). Two states fall in the region between the two ^{16}O doublets (see Fig. 3). The first has $E_x = 10.808(20)$ MeV and the second has $E_x = 10.953(25)$ MeV.

Giesen *et al.* [7] and Giesen [18] studied the ^{22}Ne$(^6$Li$, d)^{26}$Mg reaction with a relatively poor resolution of 120 keV in their deuteron spectra. In contrast, for the present experiment the energy resolution was 63 keV in the region of interest, as a result of using a solid target. We observed two ^{26}Mg states outside of the region of interest. The first, at $E_x = 9.32(6)$ MeV, corresponds to the $E_x = 9.404(20)$ MeV state of Giesen *et al.*, while the second, observed at $E_x = 9.57(4)$ MeV, is in agreement to their state at $E_x = 9.586(20)$ MeV.

A state at $E_x = 10.694(20)$ MeV was not observed in our experiment, which is consistent with the $\theta_{\text{lab}} = 7.5^\circ$ spectrum of Giesen [18]. There he reports a cross section more than one order of magnitude smaller than that of the $E_x = 10.949(25)$ MeV state at the same angle; no peak corresponding to the $E_x = 10.694(20)$ MeV state in ^{26}Mg can be identified in the spectrum. Nevertheless, one single broad peak was observed at a higher excitation energy [$E_x = 10.949(25)$ MeV]. With improved resolution we have resolved this peak into two ^{26}Mg states. It is thus likely that the spectroscopic factor for this doublet gets contributions from both states, one of them [the state with $E_x = 10.808(20)$ MeV] is at an energy too low ($E_{\text{c.m.}} = 0.193$ MeV) to contribute significantly to the reaction rate of ^{22}Ne$(\alpha,\gamma)^{26}$Mg in the region of astrophysical interest.

We identify these two states as follows: Walkiewicz *et al.* [19] studied the secondary γ-rays from thermal neutron capture for ^{26}Mg and observed an 8996.5 keV transition to the first excited state (2^+) of ^{26}Mg. They report a state with $E_x = 10.8059(4)$ MeV and Endt [11] assigned $J^\pi = (0^+ - 4^+)$ to it. This is consistent with our state at $E_x = 10.808(20)$ MeV. The ^{22}Ne$(^6$Li$, d)^{26}$Mg reaction most likely populates states with natural parity, so we propose this state to have $J^\pi = 0^+, 1^-, 2^+, 3^-$, or 4^+.

Giesen *et al.* suggested the $E_x = 10.694(20)$ MeV state to have $J^\pi = 7^-, 8^+$, or 4^+. Glatz *et al.* [20] observed this same state to decay by γ-ray emission to the $J^\pi = 5^+$ state at $E_x = 7.395(1)$ MeV. Most likely, this decay corresponds to an $M1$ transition. This is in agreement with the $J^\pi = 4^+$ assignment suggested by Karakas *et al.* [10].

An $E_x = 10.81(6)$ MeV ^{26}Mg state was reported by Crawley *et al.* [21] as well. They measured forward-angle cross sections for 201 MeV proton inelastic scattering and observed a forward-peaked angular distribution, thus suggesting $J^\pi = 1^+$. This state would not have been observed in the present experiment and most likely corresponds to the $E_x = 10.824(3)$ MeV state observed by Moss [22] and listed in Endt [11].

Our $E_x = 10.953(25)$ MeV state is at an energy consistent with the $E_x = 10.945(3)$ MeV level listed in Endt [11]. The state at $E_x = 10.953(25)$ MeV was also observed by Giesen *et al.* [7] and they suggested $J^\pi = 3^-$ without being able to discard the $J^\pi = 2^+$ and 4^+ assignments. Glatz *et al.* [20] also observed this state to decay by γ-ray emission to the $E_x = 8.625(1)$ MeV, 9.169(1) MeV, and 9.383(1) MeV states with branching ratios 29(4), 61(5), and 10(2), respectively. Endt [11] lists the three final states to have $J^\pi = 5^-, 6^-$, and 6^+, respectively. Giesen *et al.*'s J^π assignments are not consistent with these γ-ray decays. Assuming our experimental work populated natural parity states in ^{26}Mg, only $J^\pi = 5^-, 6^+$, or 7^- are allowed. The discrepancy between these results and Giesen *et al.*'s probably comes from the fact that their DWBA analysis and J^π assignment were performed for a peak consisting of two unresolved states.

We calculated the contributions from the two resolved resonances to the (α,γ) rate by taking the total differential cross section observed by [7] for their $E_x = 10.949(25)$ MeV state and splitting it into two parts. The ratio of the two contributions was taken to be equal to the ratio of the areas under the peaks observed in our deuteron spectrum (Fig. 3) after correcting for the background from ^{27}Al, as shown in Fig. 5. The spectroscopic factor S_α for each contribution was calculated by assuming a combination of spin pairs and then by fitting a DWBA model computed with the code DWUCK4 [24] to the individual experimental cross sections. For the state at $E_x = 10.808(20)$ MeV, $S_\alpha = 1.9 \times 10^{-2}$, while at $E_x = 10.953(25)$ MeV, $S_\alpha = 2.8 \times 10^{-3}$. The upper limit of the reaction rate was evaluated by assigning the states at $E_x = 10.808(20)$ MeV and $E_x = 10.953(25)$ MeV as $J^\pi = 0^+$ and $J^\pi = 5^-$, respectively. For the lower limit we took $J^\pi = 4^+$ and $J^\pi = 7^-$, respectively.

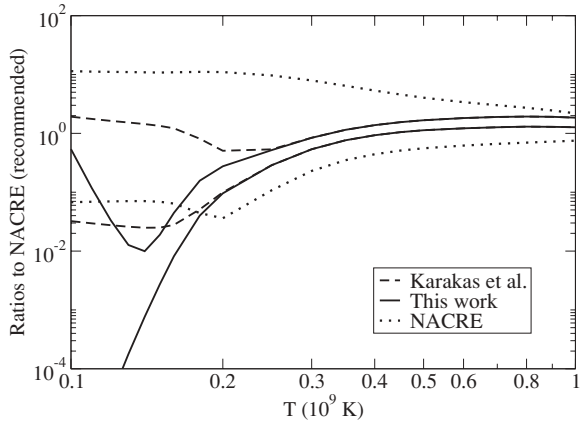

FIG. 6. Ratio of upper and lower limits to the NACRE recommended rate [23] for the ^{22}Ne$(\alpha,\gamma)^{26}$Mg reaction, as calculated by Karakas *et al.* [10] and this work.

Comparisons of our rates and the rates calculated by Karakas *et al.* [10] to NACRE [23] are shown in Fig. 6. Relative to the NACRE rates, the main effect is a reduction of the rate for temperatures below 0.3 GK. Thus an increase in the neutron production by the (α, n) reaction may be expected in these stellar environments. Nevertheless, it is necessary to finalize the spin-parity assignment of all ^{26}Mg states contributing to the (α, γ) rate and that are located below the neutron threshold. Further experimental studies are under way.

ACKNOWLEDGMENTS

We wish to thank Adam Cottrel of the University of North Carolina and Dr. Chris Westerfeldt of TUNL for their valuable help in bringing the ion implanter back in operation. We also thank the staff at Yale University's WNSL for providing the ^{6}Li beam. C.U. thanks the Yale group for their nice hospitality during visits to their laboratory.

[1] R. D. Hoffman, S. E. Woosley, and T. A. Weaver, Astrophys. J. **549**, 1085 (2001).
[2] O. Straniero, R. Gallino, M. Busso, A. Chieffi, C. M. Raiteri, M. Limongi, and M. Salaris, Astrophys. J. Lett. **440**, L85 (1995).
[3] L. S. The, M. F. El Eid, and B. S. Meyer, Astrophys. J. **655**, 1058 (2007).
[4] S. E. Woosley, A. Heger, and T. A. Weaver, Rev. Mod. Phys. **74**, 1015 (2002).
[5] M. Jaeger, R. Kunz, A. Mayer, J. W. Hammer, G. Staudt, K. L. Kratz, and B. Pfeiffer, Phys. Rev. Lett. **87**, 202501 (2001).
[6] H. W. Drotleff, A. Denker, H. Knee, M. Soiné, G. Wolf, J. W. Hammer, U. Greife, C. Rolfs, and H. P. Trautvetter, Astrophys. J. **414**, 735 (1993).
[7] U. Giesen, C. P. Browne, J. Görres, S. Graaff, C. Iliadis, H. P. Trautvetter, M. Wiescher, W. Harms, K. L. Kratz, B. Pfeiffer *et al.*, Nucl. Phys. **A561**, 95 (1993).
[8] V. Harms, K. L. Kratz, and M. Wiescher, Phys. Rev. C **43**, 2849 (1991).
[9] K. Wolke, H. W. Harms, J. W. Becker, J. W. Hammer, K. L. Kratz, C. Rolfs, U. Schröder, H. P. Trautvetter, M. Wiescher, and A. Wöhr, Z. Phys. A **334**, 491 (1989).
[10] A. I. Karakas, M. A. Lugaro, M. Wiescher, J. Görres, and C. Ugalde, Astrophys. J. **643**, 471 (2006).
[11] P. M. Endt, Nucl. Phys. **A633**, 1 (1998).
[12] P. E. Koehler, Phys. Rev. C **66**, 055805 (2002).
[13] H. W. Fulbright, Annu. Rev. Nucl. Part. Sci. **29**, 161 (1979).
[14] L. Rowton, *Proceedings of SNEAP-XXVIII*, Western Michigan University, Oct. 12–15, 1994 (World Scientific, Singapore, 1995), pp. 13–15.
[15] A. Parikh, Ph.D. thesis, Yale University (2006).
[16] D. Shapira, R. M. DeVries, H. W. Fulbright, J. Tōke, and M. R. Clover, Nucl. Instrum. Methods **129**, 123 (1975).
[17] R. B. Firestone *et al.*, *Table of Isotopes* (Wiley Interscience, New York, 1996).
[18] U. Giesen, Ph.D. thesis, University of Notre Dame (1992).
[19] T. A. Walkiewicz, S. Raman, E. T. Jurney, J. W. Starner, and J. E. Lynn, Phys. Rev. C **45**, 1597 (1992).
[20] F. Glatz, S. Norbert, E. Bitterwolf, A. Burkard, F. Heidinger, T. Kern, R. Lehmann, H. Röpke, J. Siefert, C. Schneider *et al.*, Z. Phys. A **324**, 187 (1986).
[21] G. M. Crawley, C. Djalali, N. Marty, M. Morlet, A. Willis, N. Anantaraman, B. A. Brown, and A. Galonsky, Phys. Rev. C **39**, 311 (1989).
[22] C. E. Moss, Nucl. Phys. **A269**, 429 (1976).
[23] C. Angulo *et al.*, Nucl. Phys. **A656**, 3 (1999).
[24] P. D. Kunz, program DWUCK4, extended version by J. Comfort (unpublished, 1983).